



**AALBORG UNIVERSITY**  
DENMARK

**Aalborg Universitet**

## **Stability analysis and active damping for LLCL-filter based grid-connected inverters**

Huang, Min; Blaabjerg, Frede; Loh, Poh Chiang; Wu, Weimin

*Published in:*

Proceedings of the 2014 International Power Electronics Conference (IPEC-Hiroshima 2014 - ECCE-ASIA)

*DOI (link to publication from Publisher):*

[10.1109/IPEC.2014.6869958](https://doi.org/10.1109/IPEC.2014.6869958)

*Publication date:*

2014

*Document Version*

Early version, also known as pre-print

[Link to publication from Aalborg University](#)

*Citation for published version (APA):*

Huang, M., Blaabjerg, F., Loh, P. C., & Wu, W. (2014). Stability analysis and active damping for LLCL-filter based grid-connected inverters. In *Proceedings of the 2014 International Power Electronics Conference (IPEC-Hiroshima 2014 - ECCE-ASIA)* (pp. 2610-2617). IEEE Press. <https://doi.org/10.1109/IPEC.2014.6869958>

### **General rights**

Copyright and moral rights for the publications made accessible in the public portal are retained by the authors and/or other copyright owners and it is a condition of accessing publications that users recognise and abide by the legal requirements associated with these rights.

- Users may download and print one copy of any publication from the public portal for the purpose of private study or research.
- You may not further distribute the material or use it for any profit-making activity or commercial gain
- You may freely distribute the URL identifying the publication in the public portal -

### **Take down policy**

If you believe that this document breaches copyright please contact us at [vbn@aub.aau.dk](mailto:vbn@aub.aau.dk) providing details, and we will remove access to the work immediately and investigate your claim.

# Stability Analysis and Active Damping for *LLCL*-filter Based Grid-Connected Inverters

Min Huang, Frede Blaabjerg, Poh Chiang Loh  
 Department of Energy Technology  
 Aalborg University  
 Aalborg, Denmark  
[hmi@et.aau.dk](mailto:hmi@et.aau.dk), [fbl@et.aau.dk](mailto:fbl@et.aau.dk), [pcl@et.aau.dk](mailto:pcl@et.aau.dk)

Weimin Wu  
 Electrical Engineering  
 Shanghai Maritime University  
 Shanghai, China  
[wmwu@cle.shmtu.edu.cn](mailto:wmwu@cle.shmtu.edu.cn)

**Abstract**— A higher order passive power filter (*LLCL*-filter) for the grid-tied inverter is becoming attractive for the industrial applications due to the possibility to reduce the cost of the copper and the magnetic material. To avoid the well-known stability problems of the *LLCL*-filter it is requested to use either passive or active damping methods. This paper analyzes the stability when damping is required and when damping is not necessary considering sampling and transport delay. Basic *LLCL* resonance damping properties of different feedback states are also studied. Then an active damping method which is using the capacitor current feedback for *LLCL*-filter is introduced. Based on this method, a design procedure for the control method is given. Last, both simulation and experimental results are provided to validate the theoretical analysis of this paper.

**Keywords**— *LLCL*-filter, grid converter, active damping, current control, resonant frequency, stability.

## I. INTRODUCTION

Recently, due to the energy crisis, distributed generation (DG) systems using clean renewable energy such as solar energy, wind energy, etc., have become an important issue in the technical research. Typically, a simple series inductor  $L$  is inserted between a voltage source inverter (VSI) and the grid to attenuate the high-frequency PWM harmonics to a desirable limit. But the high value of  $L$ -filter needs to be adopted to reduce the current harmonics around the switching frequency, which would lead to a poor dynamic response of the system and a high power loss. Hence, a low-pass passive power filter, *LCL*-filter, can achieve a high harmonic attenuation performance with less total inductance ( $L_1 + L_2$ ) [1], [2].

In order to further reduce the total inductance, the *LLCL*-filter was proposed [3]. Compared with the *LCL*-filter, the total inductance and volume of the *LLCL*-filter can be reduced a factor of 25% ~40%. So, the *LLCL*-filter for the grid-tied inverter is becoming attractive for industrial applications [4]. The application of *LLCL*-filter for a three-phase three-wire Shunt Active Power Filter (SAPF) [5] and a Large-Scale Wave Power Plant [6] were analyzed.

As a high order filter, the *LLCL*-filter has also a resonant problem. To suppress the possible resonances of an *LCL*-filter or *LLCL*-filter, active damping [7-11] or passive damping [12-15] measures may be adopted. Passive damping is realized by adding additional components in the system but it causes a decrease of the overall system efficiency. For a stiff grid application, a

passive damping strategy is more attractive. Due to high efficiency and flexibility, the active damping method might be preferred, although at the risk of higher cost of sensors and more control complexity. Normally, the digital sampling and transport delays caused by the controller and modulation, as well as discretization effects are taken into account. The delay will influence the stability of the system and when resonant frequency varies, active damping is usually required in an *LCL*-filter [8].

Proportional Resonant (PR) compensator and Proportional Integral (PI) compensator are widely used to control the injected grid current in single-phase grid-connected inverters [16]-[18]. The converter control commonly consists of an outer dc-link voltage PI control loop and an inner current control loop. In this paper, all possible feedback states of currents and voltages of *LLCL*-filter capacitors and inductors with different feedback transfer functions are considered and compared in the continuous Laplace domain. The results show how the various feedback signals need to be fed back in order to achieve resonance damping. Based on the available choices of feedback variables, active damping of the capacitor current control strategy is used for *LLCL*-filter.

First, the system is described and its stability is analyzed in Section II. In Section III, a more general analysis of different active resonance damping solutions is carried out. The basic *LLCL* resonance damping properties of different feedback states are studied. In Section IV, the design of current controller and capacitor current feedback damping are described. Last, a 6-kW three-phase grid-connected inverter is built to verify the proposed design method.

## II. MODELING AND STABILITY OF *LLCL*-FILTER-BASED GRID-CONNECTED INVERTER

### A. Modeling of *LLCL*-filter-based Grid-connected Inverter

A three-phase voltage source converter connected to the grid via an *LLCL*-filter is studied as shown in Fig. 1. The inverter output voltage and current are represented as  $u_i$  (phase voltage) and  $i_c$ , and the grid voltage and current are represented as  $u_g$  and  $i_g$ .  $L_g$  is the grid impedance. Grid side current control will be discussed in this paper [1].

Neglecting the influence of the grid impedance and Equivalent Series Resistances (ESRs) of the inductors and capacitors, the transfer function  $i_g(s) / u_i(s)$  of the *LLCL*-filter can be derived in (1).

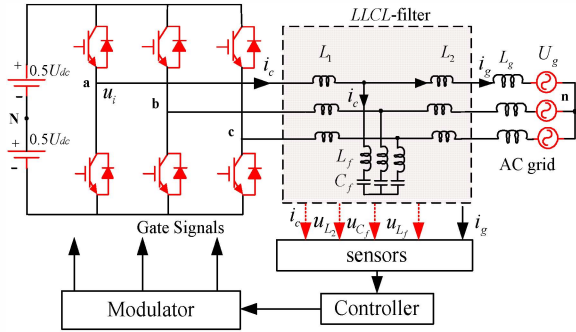


Fig. 1. General structure of three-phase grid-connected inverter with *LLCL*-filter.

$$G_{u_i \rightarrow i_g}(s) = \frac{L_f C_f s^2 + 1}{(L_1 L_2 C_f + (L_1 + L_2) L_f C_f) s^3 + (L_1 + L_2) s} \quad (1)$$

$$\omega_r = \frac{1}{\sqrt{\left(\frac{L_1 L_2}{L_1 + L_2} + L_f\right) C_f}} \quad (2)$$

As shown in (2),  $\omega_r$  is the resonant frequency (in radians per second),  $f_r$  is the resonant frequency. If the inductance of  $L_f$  is set to zero, then the transfer functions of the *LCL*-filter can also be calculated. Fig. 2 shows bode plots of transfer functions  $i_g(s) / u_i(s)$  of *LCL*-filter and *LLCL*-filter when they meet the same harmonic requirement of grid-injected current according to IEEE 519-1992[19].

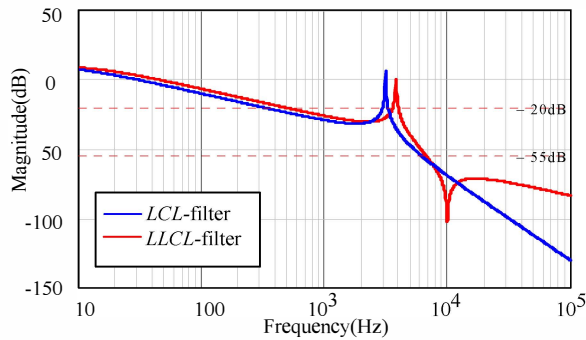


Fig. 2. Bode plots of transfer functions  $i_g(s) / u_i(s)$  for different filters.

It can be seen from Fig. 2, the resonant frequency of the *LLCL*-filter is higher than the resonant frequency of the *LCL*-filter. The ratio of the resonant frequency and the sampling frequency is relative to the stability of *LCL*-filter due to the delay. It means that if an *LCL*-filter with a low resonance frequency is chosen for the purpose of high damping of switching harmonics, the design of the active damping gets very difficult and a poor robustness is obtained [11], [20], and [21]. For the *LLCL*-filter, the ratio of the resonant frequency and the sampling frequency also influence the control and stability.

Table I shows the parameters of the selected test system. Table II shows the parameters of the *LLCL*-filter in different resonant frequencies cases according to the design method given in [19].

### B. Stability of *LLCL*-Filter-Based Grid-Connected Inverter with Different Resonant Frequencies

The inverter can be modeled as a linear gain  $k_{PWM}$ . The control block diagram of a single loop controller without any damping methods of the three-phase grid-connected inverter with *LLCL*-filter is shown in Fig. 3.

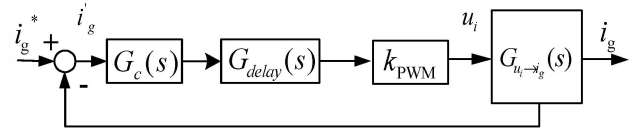


Fig. 3. Block diagram of grid current feedback control.

Other transfer functions in Fig. 3 are shown in (3)-(4) in  $s$ -domain.  $G_c(s)$  is a PI controller, where  $k_p$  and  $\tau$  are representing its proportional gain, integral time constant respectively.  $G_{delay}(s)$  is the delay part in series with the forward path. One sample period delay due to computation and PWM are included.  $G(s)$  is the open transfer function of the grid current feedback control.

$$G_c(s) = k_p + \frac{k_p}{s\tau} \quad (3)$$

$$G(s) = G_{delay}(s) k_{PWM} G_c(s) G_{u_i \rightarrow i_g}(s) \quad (4)$$

TABLE I  
Test System Parameters

DC link voltage $U_{dc}$	700 V	Grid frequency $f_o$	50 Hz
Grid phase voltage $U_g$	220 V	Sample frequency $f_d$	10kHz
Switching frequency $f_s$	10kHz	Sampling period $T_s$	100 us

TABLE II  
*LLCL*-filter Parameters and Resonance Frequency

Case I	Case II	Case III
$L_1=2.4\text{mH}$	$L_1=2.4\text{mH}$	$L_1=3\text{mH}$
$L_2=1.2\text{mH}$	$L_2=2\text{mH}$	$L_2=2.4\text{mH}$
$C_f=2\mu\text{F}$	$C_f=8\mu\text{F}$	$C_f=8\mu\text{F}$
$L_f=128\mu\text{F}$	$L_f=32\mu\text{F}$	$L_f=32\mu\text{F}$
$f_r=3.69\text{kHz}$	$f_r=1.68\text{kHz}$	$f_r=1.523\text{kHz}$
$f_r/f_d=0.369$	$f_r/f_d=0.168$	$f_r/f_d=0.153$

Fig. 4 shows the bode plot of the forward path transfer function for the single loop.

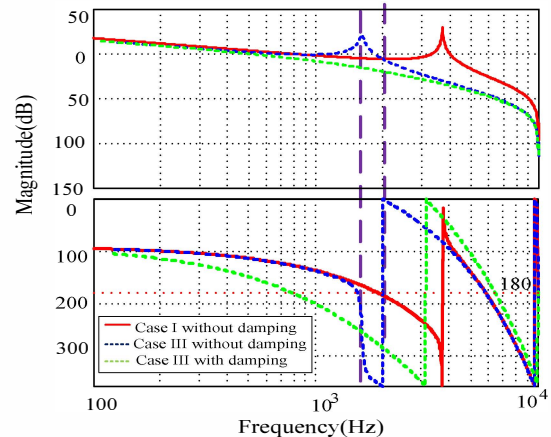


Fig. 4. Bode plot of the forward path transfer function for the single loop shown in Fig. 3.

It can be seen from Fig. 4, that the *LLCL*-filter resonance has no influence on system stability when the resonant frequency is high, since the phase is already well below  $-180^\circ$  due to the sampling and transport delay.

This analysis identifies that there is also a resonant frequency critical for *LLCL*-filter, and above it, active damping can be avoided by adjusting the controller gain. When a Zero-Order-Hold (ZOH) is in series of the open loop, discretization of the system introduces delay too, as shown in (5).

$$G_0(s) = H_o(s)G_{u_i \rightarrow i_g}(s) = (1 - e^{-T_d s}) \frac{G_{u_i \rightarrow i_g}(s)}{s} \quad (5)$$

When  $\angle G(j\omega_k) = -\pi$ , the function is shown in (6).  $\omega_k = \pi/3T_d$ , it is the root. If a phase angle is already below  $-180^\circ$  at this resonant frequency, the system can be stable. It can also deduce that  $f_k = f_d/6$ ,  $f_k$  is the critical frequency.

Hence, a single loop is sufficient to be stable when the resonant frequency is above the critical frequency and active damping is necessary when the resonant frequency is below the critical frequency. For the example in Table I, the critical frequency  $f_k$  is 1.68 kHz.

$$\angle G(j\omega_k) = \angle \left\{ \frac{e^{-j\omega_k T_d} \cdot \frac{1 + j\omega_k \tau}{j\omega_k \tau} \cdot \frac{1 - e^{-j\omega_k T_d}}{j\omega_k}}{1 - L_f C_f \omega_k^2} \right\} = -\pi$$

$$\left. \frac{j[(L_1 + L_2)\omega_k - (L_1 L_2 C_f + (L_1 + L_2)L_f C_f)\omega_k^3]}{1 - L_f C_f \omega_k^2} \right\} = -\pi \quad (6)$$

Fig. 5 shows the closed loop root loci of the three cases in Table II for the single loop grid current feedback.

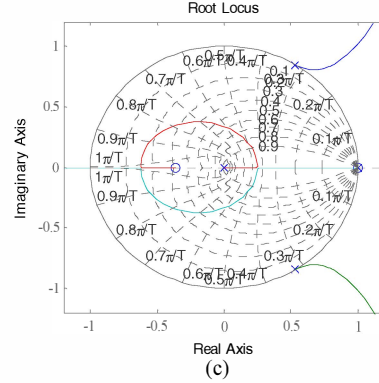
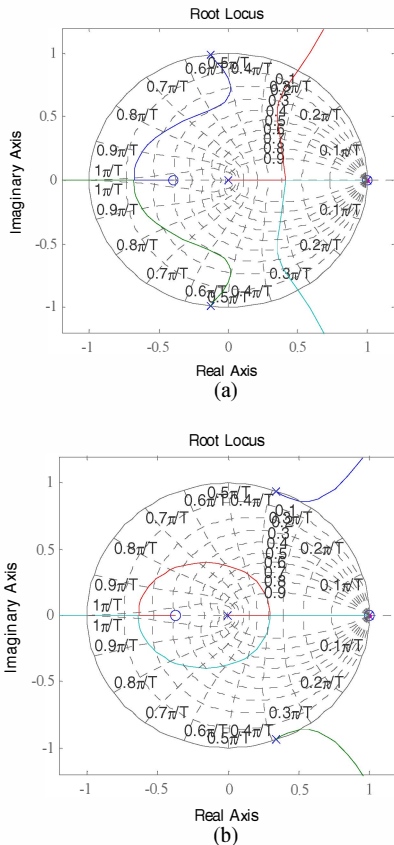


Fig. 5. Root loci of grid current feedback (without damping) of different cases in Table II. (a) Case I, (b) Case II and (c) Case III.

Fig. 5 (a) depicts the *LLCL* resonant frequency is above the critical frequency. The poles initially track inside the unit circle with the proper proportional gain  $K_p$ . Fig. 5(b) shows the *LLCL* resonant frequency at the critical frequency. The system is on the edge to be unstable. When the resonant frequency is less than the critical frequency system will always be unstable regardless of what the proportional gain is without damping, as shown in Fig. 5(c). In this case, a damping method is necessary to be used.

### III. STUDY OF ACTIVE DAMPING WITH DIFFERENT FEEDBACK STATES

#### A. Notch Filter Concept

Active damping methods can be classified into two main classes: multi-loop and filter-based active damping [8]. For passive damping, the resonance frequency of an *LCL*-filter can be damped by connecting a resistor to the filter. The virtual resistance without reducing the efficiency was introduced, which is the equivalent as the passive damping resistors of the filter that resonance damping techniques.

The control structure of inner current loop with a notch concept [22] is shown in Fig. 6.

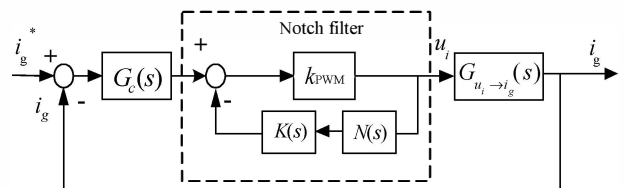


Fig. 6. Active damping based on a notch filter concept.

$$B(s) = \frac{k_{PWM}}{1 + k_{PWM} K(s)N(s)} = \frac{s^2 + \omega_r^2}{s^2 + 2\xi\omega_r s + \omega_r^2} \quad (7)$$

In order to eliminate the resonant peak at the frequency  $\omega_r$ , the notch  $B(s)$  should have a negative peak in  $\omega_r$ , so it can be expressed as (7).

There are different variables can be chosen as control object for *LLCL*- of detection variables, it has different function  $K(s)$  with different feedback variables. Table III shows the expressions filter. The structure of  $N(s)$  depends on the selection using the filter capacitor voltage  $u_{cs}$ , filter capacitor current  $i_c$ , filter resonant inductor

voltage in grid side  $u_{L_2}$ , inductor voltage in resonant circuit  $u_{L_r}$ . It can be seen from the Table III, the feedback function of grid side inductor voltage is a little complex. The choice of the sensor location depends strongly on the application situations. For different ratios between the resonance frequency and control frequency, the selected approaches behave differently [10].

### B. Filter Capacitor Current Feedback

For the *LCL*-filter, capacitor current feedback and capacitor voltage feedback are often used [10]. When the capacitor current feedback is sensed,  $K(s)$  can be easily configured as a proportion link, which is isolated with the system parameters. Fig. 7 shows the capacitor current feedback control scheme according to Fig. 6.

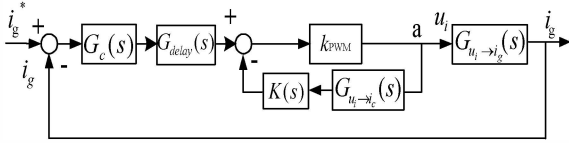


Fig.7. Capacitor current feedback control scheme.

$$N(s) = G_{u_i \rightarrow i_c}(s) = \frac{\omega_r^2 L_2 C_f s}{(s^2 + \omega_r^2)(L_1 + L_2)} \quad (8)$$

Then the open loop transfer function of the capacitor current feedback control from  $i_g$  to  $i_g^*$  is shown in (9)

$$G(s)_{open} = \frac{k_{PWM} \omega_r^2 (L_f C_f s^2 + 1) G_c(s) G_{delay}(s)}{(s^2 + \omega_r^2)(L_1 + L_2) + K_{i_c} G_{delay}(s) k_{PWM} L_2 s \omega_r^2} \frac{1}{s} \quad (9)$$

As shown in Fig. 4, the capacitor current feedback can dampen the resonant peak and make the system stable.

### C. Filter Capacitor Voltage Feedback

When the capacitor voltage is sensed, a derivative filter capacitor voltage feedback is required for the resonance damping. Some papers have illustrated this method for an *LCL*-filter. As shown in Table III, a differential feedback is necessary but it may cause noise problems in the control because it will amplify high-frequency signals [23].

### D. Filter Resonant Inductor Voltage Feedback

When the resonant inductor voltage is sensed, the integral feedback can be expected to keep the system stable. Normally, the filter capacitor current is sensed for the *LCL*-filter but the voltage sensor is cheaper than current sensor. This is a new active damping method for *LLCL*-filter which can reduce the cost of sensor. The resonant inductor voltage feedback can also be transferred in Fig. 7. The feedback coefficient is integral and the structure of  $N(s)$  is the transfer function from  $u_i$  to  $u_{L_r}$ .

The next section will analyze the design of capacitor current feedback only.

TABLE III  
TRANSFER FUNCTIONS OF DIFFERENT VARIABLES FEEDBACK

Variable	$u_{C_f}$	$i_c(s)$	$u_{L_f}(s)$	$u_{L_2}$
$N(s)$	$\frac{\omega_r^2 L_2}{(s^2 + \omega_r^2)(L_1 + L_2)}$	$\frac{\omega_r^2 L_2 C_f s}{(s^2 + \omega_r^2)(L_1 + L_2)}$	$\frac{\omega_r^2 L_2 L_f C_f s^2}{(s^2 + \omega_r^2)(L_1 + L_2)}$	$\frac{\omega_r^2 L_2 (L_f C_f s^2 + 1)}{(s^2 + \omega_r^2)(L_1 + L_2)}$
$K(s)$	$s K_{u_{C_f}}$	$K_{i_c}$	$\frac{K_{u_{L_f}}}{s}$	$K_{u_{L_2}} \frac{C_f s}{L_f C_f s^2 + 1}$

## IV. DESIGN OF CURRENT REGULATOR AND CAPACITOR CURRENT FEEDBACK COEFFICIENT

### A. PI Controller Gain Design

The maximum possible controller gains for the system can now be analytically determined using the concepts developed in [24] - [26]. The proportional gain is then set to achieve unity gain at the desired crossover frequency  $f_c / \omega_c$ . The choice of  $k_p$  can be decided by the system bandwidth satisfying the desired phase margin  $\Phi_m$ . For a single loop control, the phase angle at the crossover frequency can be described in (10). In addition, the crossover frequency  $\omega_c$  can be determined, when the *LCL*-filter is approximated to an *L*-filter.

$$\omega_c = \frac{\pi / 2 - \Phi_m}{3T_d / 2} \quad (10)$$

Usually, the integral time constant  $\tau$  can be set as  $10/\omega_c$ .

The system open-loop gain achieves unity at  $\omega_c$ . Then the maximum gain can be calculated as

$$|\angle G(j\omega_c)| \approx \left| \frac{k_p \sqrt{(\omega_c \tau)^2 + 1}}{\omega_c \tau} \right| \left| \frac{1 - e^{-j\omega_c T_d}}{j\omega_c} \right| \left| \frac{k_{PWM}}{j(L_1 + L_2)\omega_c} \right|$$

$$k_p \approx \frac{\omega_c (L_1 + L_2)}{k_{PWM}} \quad (11)$$

### B. Capacitor current Feedback Coefficient Gain

The denominator of closed loop transfer function of *LLCL*-filter is shown in (12) based on (9). Base on (12) the minimum value of  $K_{i_c}$  can be found using the limiting ratio of proportional gain  $k_p$  to dampen using Routh's Stability Criterion, as shown in (13).

$$D(s) = [L_1 L_2 C_f + (L_1 + L_2) L_f C_f] s^4 + K_{i_c} k_{PWM} L_f L_2 C_f s^3 + (L_1 + L_2) s^2 + k_p k_{PWM} s + k_p k_{PWM} / \tau \quad (12)$$

$$K_{ic} \geq \frac{k_p}{(L_1 + L_2)L_2} [L_1L_2 + (L_1 + L_2)L_f] \quad (13)$$

$GM_1$  and  $GM_2$  are defined by the magnitude of (9) at  $f_r$ , and  $f_d/6$  [27]. Then the limitation of  $K_{ic}$  can be obtained from (14) and (15).

$$K_{ic} = 10^{GM_1/20} \frac{2\pi f_c L_1}{k_{PWM}} \quad (14)$$

$$K_{ic} = 10^{GM_2/20} \left(\frac{6f_c}{f_d}\right)^2 \frac{2\pi f_c L_1}{k_{PWM}} + \frac{2\pi f_c L_1}{k_{PWM}} \frac{(f_d/6)^2 - (f_r)^2}{f_d/6} \quad (15)$$

$K_{ic}$  should satisfy this region. Hence, the basic design procedures can be addressed as:

1. Determine the specifications of the loop gain. Desired phase margin  $\Phi_m$  is  $40^\circ$ ,  $GM_2$  is 5.1 dB, and  $GM_1$  is  $-5.8$  dB.
2. Obtain the value of  $k_p$  and  $f_c$  to satisfy all the requirements according to (10), (11) and (13),  $f_c = 1.1$  kHz is chosen to obtain fast dynamic response. Then  $k_p$  is calculated according to (11).
3. Taking  $f_c = 1.1$  kHz in (13), (14) and (15), calculate the satisfactory feedback gain in this example.

Fig. 8 shows the loci branches of the system with the capacitor current coefficient increasing. There is a stable range of  $K_{ic}$  as shown in Fig. 8. The calculated gain should not pass the limitation.

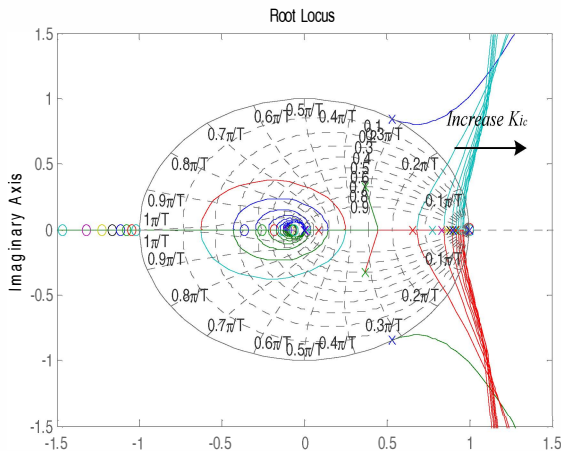


Fig.8. Root loci of the system with  $K_{ic}$  increasing.

## V. SIMULATION AND EXPERIMENTAL RESULTS

### A. Simulation Results

In order to illustrate the stability and verify the active damping method of *LLCL*-filter based grid-connected inverter, a three-phase inverter with 6 kW rated power is simulated using MATLAB. This paper uses a PI controller and SVPWM modulation. The detailed system parameters are listed in Table I and Table II.

First, in order to investigate stability of the system without damping in different resonant frequencies, the *LLCL*-filter is analyzed into three cases with different parameters, one with a high resonance frequency, one with a critical resonance frequency and the other with a

low resonance frequency. According to (11), the controller gain is  $k_p = 0.065$  and  $\tau = 1.59$  ms.

(1) Case I: high frequency,  $f_{res} = 3.69$  kHz.

In the case I, the resonant frequency is high (3.69 kHz) and crossover frequency is set to 1.1 kHz in order to get a fast response and to meet phase margin limitation. It can be seen from Fig. 9 the system is stable.

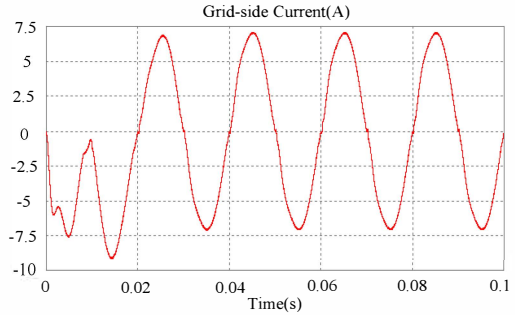


Fig. 9. Grid-side current waveform of Case I ( $f_{res} = 3.69$  kHz).

(2) Case II: critical frequency  $f_{res} = 1.68$  kHz.

As it mentioned before, there is a critical frequency for *LLCL*-filter. It is calculated as  $f_d/6$  based on the function (6). It can be seen from Fig. 10, the system is almost unstable at the critical frequency. When the grid impedance is increased, the resonant frequency will be deduced more.

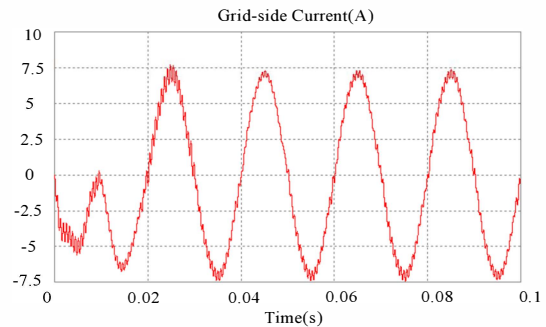


Fig. 10. Grid-side current waveform of Case II ( $f_{res} = 1.68$  kHz).

As shown in Fig. 11, when the grid impedance is set to 2.4 mH, the resonant frequency is reduced to 1.6 kHz which is under the critical frequency and the system is unstable.

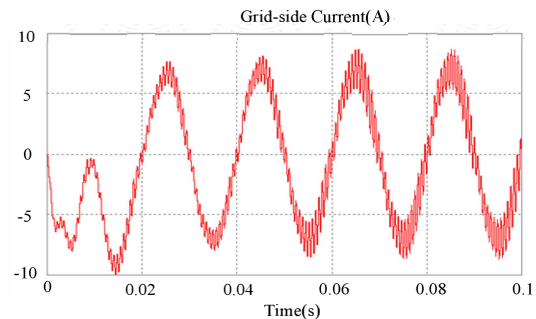


Fig. 11. Grid-side current waveform of Case II when Increase  $L_2$  to 2.4 mH ( $f_{res} = 1.60$  kHz).

As shown in Fig. 12, when the grid-side inductance is set to 1.2 mH, the resonant frequency is increased to 1.95 kHz and the system is changed from critical state to stable.

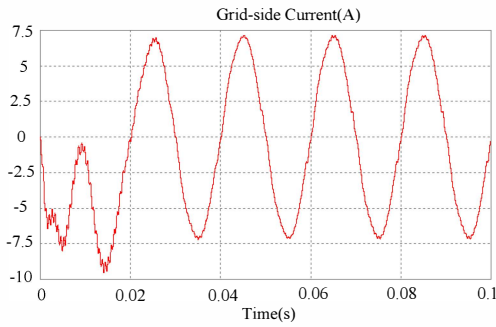


Fig. 12. Grid-side current waveform of Case II when increase  $L_2$  to 2.4mH ( $f_{res}=1.95$  kHz).

(3) Case III: Low frequency  $f_{res}=1.523$  kHz

In case III, the resonant frequency is low (1.523 kHz). It can be seen from Fig. 13 that system is completely unstable without damping.

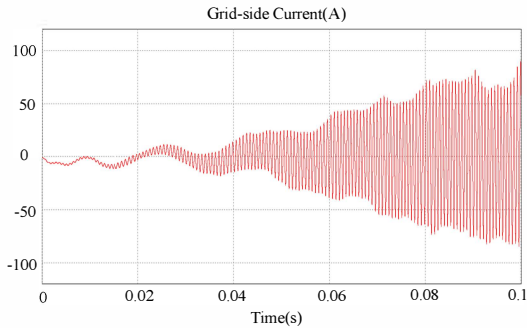


Fig. 13. Grid-side current waveform of Case III ( $f_{res}=1.523$  kHz).

So, when designing the parameters it is better to make the resonant frequency higher in order to get a better stability and robustness. When the resonant frequency is lower or nearby the critical frequency, the active damping method is necessary to be used. In this paper, take Case III as an example, the active damping with a capacitor current feedback is used.

Applying the parameters described in Table I and Table II, the crossover frequency is set to 1.1 kHz to get a high response and meet the phase margin limitation.

In case III, the resonant frequency is low (1.53 kHz). In order to get enough phase margin crossover frequency should be set below the resonant frequency. According to (12), the PI controller gains  $k_p = 0.043$  and  $\tau = 3.18$  ms.

Fig. 14 and Fig. 15 show the dynamic performance of Case I and Case III respectively when the reference current changes from 7 A to 12.9 A at time 0.1s to test the dynamic performance. It can be seen from Fig. 14, there is no oscillation during the transient in the high resonant frequency without damping methods. Fig. 8 shows the same dynamic performance in the low resonant frequency when the capacitor current feedback active damping method is used. It can also be seen that the current ripple in Fig. 15 is smaller than the current ripple in Fig. 14, because the inductance and capacitance in the high resonant frequency case is larger than that in the low resonant frequency case.

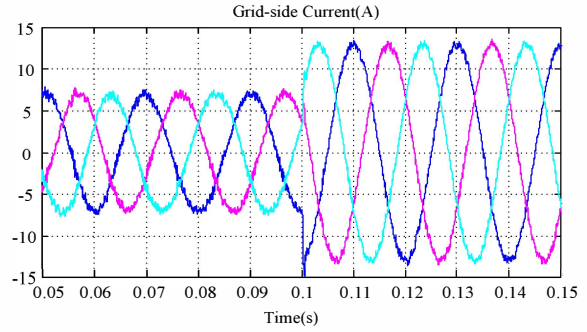


Fig. 14. Grid-side currents of Case I (high resonant frequency) without active damping.

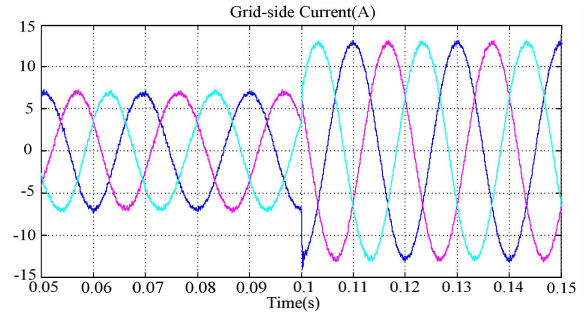


Fig. 15. Grid-side currents of Case III (low resonant frequency) with active damping.

Fig. 16 shows that the system is unstable at the beginning in low resonance frequency case, but it turns out to be stable when active damping is enabled at 0.1 in Case III. Fig.17 shows that the system becomes unstable when the value of the capacitor feedback coefficient is increased. There is a limited stable region for the feedback coefficient.

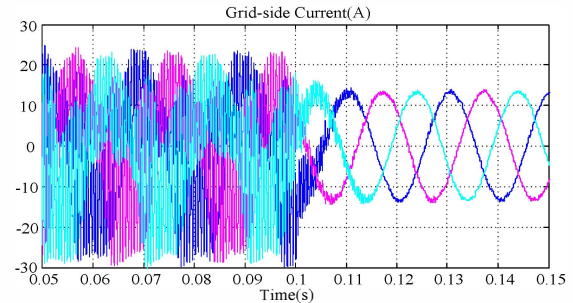


Fig. 16. Grid-side currents of Case III when active damping is enabled at time 0.1s.

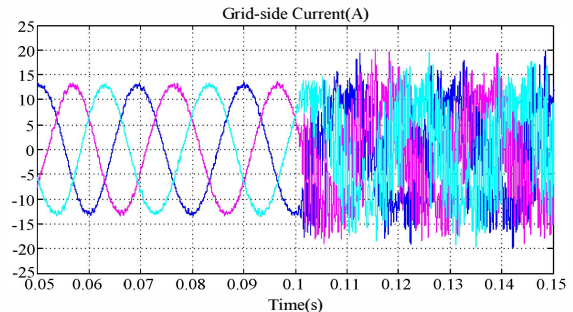


Fig. 17. Grid-side currents of Case III when  $K_{i_c}$  is increased at time 0.1s.

B. Experimental Results

The control algorithm is implemented on a dsPACE DS 1006 board. Due to the limitation of the setup, the power in experiment is lower than the simulation. Fig. 18

shows the dynamic transition of grid-side currents in high resonant frequency case when the power is increased without active damping. Fig. 19 shows the grid-side currents when active damping is enabled in the low resonant frequency case.

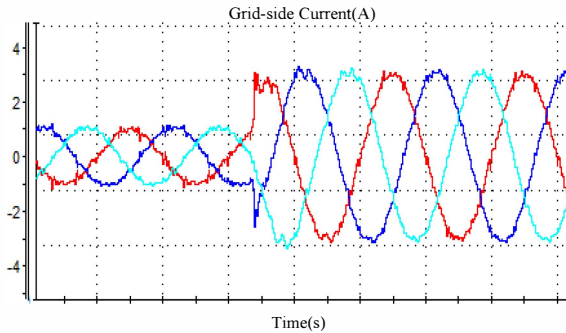


Fig. 18. Experimental grid-side currents in high resonant frequency case without active damping.

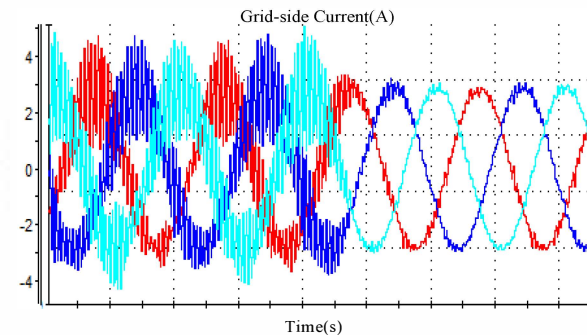


Fig. 19. Experimental grid-side currents in low resonant frequency case when active damping is enabled.

## VI. CONCLUSION

Compared with the *LCL*-filter, the resonant frequency of *LLCL*-filter is higher and it is easier to be stable. The work presented in this paper shows when damping method is not required in an *LLCL*-filter as the resonant frequency varies considering different sampling and transport delays. The critical frequency is determined by the delay time and sample frequency.

In the low resonant frequency cases, or critical cases, the resonant frequency is easy to be changed due to the parameter variation and grid impedance variation. Then, damping methods are necessary to be used. Based on the analysis of possible feedback variables, capacitor current feedback active damping control strategy is chosen for the *LLCL*-filter. Simulation and experiment results prove the influence of the resonant frequency and design of capacitor current feedback. The control of *LCL*-filter and *LLCL*-filter are similar and the additional inductor of *LLCL*-filter brings no extra control difficulties.

## REFERENCES

[1] M. Liserre, F. Blaabjerg, and S. Hansen, "Design and Control of an LCL-Filter-Based Three-Phase Active Rectifier", *IEEE Trans. Ind. Appl.*, vol. 41, no. 5, pp. 1281-1291, Sep./Oct. 2005.  
 [2] V. Salas, and E. Ollás, "Overview of the state of technique for PV inverters used in low voltage grid-connected PV systems:

Inverters above 10 kW," *Renewable Sustainable Energy Rev.*, vol. 15, no. 2, pp. 1025-1257, Feb. 2011.  
 [3] W. Wu, Y. He, and F. Blaabjerg, "An *LLCL* power filter for single-phase grid-tied inverter," *IEEE Trans. Power Electron.*, vol. 27, no. 2, pp. 782-789, Feb. 2012.  
 [4] J. M. Bloemink, T. C. Green, "Reducing Passive Filter Sizes with Tuned Traps for Distribution Level Power Electronics," in *Proc. of IEEE EPE 2011*, pp. 1-9, Aug. 2011.  
 [5] K. Dai, K. Duan, X. Wang, "Yong Kang Application of an *LLCL* Filter on Three-Phase Three-Wire Shunt Active Power Filter," in *Proc. of IEEE INTELEC 2012*, pp. 1-5, Sep. 2012.  
 [6] A. M. Cantarellas, E. Rakhshani, D. Remon, P. Rodriguez, "Design of the *LCL*+trap filter for the two-level VSC installed in a large-scale wave power plant," in *Proc. IEEE Energy Conversion Congress and Exposition (ECCE)*, pp. 707-712, 2013.  
 [7] J. Dannehl, M. Liserre and F. Fuchs, "Filter-based active damping of voltage source converters with *LCL* filters," *IEEE Trans. Ind. Electron.*, vol. 58, no. 8, pp. 3623-3633, Oct. 2011.  
 [8] M. Liserre, A. D. Aquila, and F. Blaabjerg, "Genetic algorithm-based design of the active damping for an *LCL*-filter three-phase active rectifier," *IEEE Trans. Power Electron.*, vol. 19, no. 1, pp. 76-86, Jan. 2004.  
 [9] R. Teodorescu, F. Blaabjerg, M. Liserre, and A. Dell'Aquila, "A stable three-phase *LCL*-filter based active rectifier without damping," in *Proc. 2003 IEEE Ind. Appl. Soc. Annu. Meeting*, pp. 1552-1557, 2003.  
 [10] J. Dannehl, F. Fuchs, S. Hansen, "Investigation of active damping approaches for PI-based current control of grid-connected pulse width modulation converters with *LCL* filters," *IEEE Trans. Ind. App.*, vol. 46, no. 4, pp. 1509-1517, 2010.  
 [11] S. Parker, B. McGrath, and G. Holmes, "Regions of Active Damping Control for *LCL* Filters," in *Proc. IEEE Energy Conversion Congress and Exposition (ECCE)*, Raleigh, NC, pp. 53-60, 2012.  
 [12] W. Wu, Y. He, and F. Blaabjerg, "A New Design Method for the Passive Damped *LCL*- and *LLCL*-Filter Based Single-Phase Grid-tied Inverter," *IEEE Trans. Ind. Electron.*, vol. 60, no. 10, pp. 4339-4350, Oct. 2013.  
 [13] W. Wu, M. Huang, Y. Sun, X. Wang, F. Blaabjerg, "A composite passive damping method of the *LLCL*-filter based grid-tied inverter," in *Proc. of PEDG 2012*, Aalborg, Denmark, pp: 759 - 766, 25-28 June 2012.  
 [14] R. Peña-Alzola, M. Liserre, F. Blaabjerg, R. Sebastián, J. Dannehl, F.W. Fuchs, "Analysis of the Passive Damping Losses in *LCL*-Filter-Based Grid Converters," *IEEE Power Electronics Transactions on*, vol. 28, no. 6, pp. 2642-2646, June 2013.  
 [15] P. Channegowda and V. John, "Filter Optimization for Grid Interactive Voltage Source Inverters," *IEEE Trans. on Ind. Electron.*, vol. 57, no. 12, pp. 4106-4114, Dec. 2010.  
 [16] D. G. Holmes, T. A. Lipo, B. P. McGrath and W. Y. Kong, "Optimized design of stationary frame three phase AC current regulators," *IEEE Trans. Power Electron.*, vol. 24, no. 11, pp. 2417-2425, Nov. 2009.  
 [17] D. Pan, X. Ruan, C. Bao, W. Li, X. Wang, "Capacitor-Current-Feedback Active Damping With Reduced Computation Delay for Improving Robustness of *LCL*-Type Grid-Connected Inverter Capacitor-Current-Feedback Active Damping With Reduced Computation Delay for Improving Robustness of *LCL*-Type Grid-Connected Inverter," *IEEE Trans. Power Electron.*, vol. 29, no. 7, pp. 3414-3427, 2014.  
 [18] D. Ricchiuto, M. Liserre, T. Kerekes, R. Teodorescu, F. Blaabjerg, "Robustness analysis of active damping methods for an inverter connected to the grid with an *LCL*-filter", in *Proc. of Energy Conversion Congress and Exposition (ECCE)*, on page(s): 2028 - 2035, 2011.  
 [19] M. Huang, W. Wu, F. Blaabjerg, and Y. Yang, "Step by Step Design of a High Order Power Filter for Three-Phase Three-Wire Grid-connected Inverter in Renewable Energy System," in *Proc. of PEDG 2013*, pp. 1-8, July 08-11, 2013.  
 [20] S. Yang, Q. Lei, P. F.Z., Z. Qian, "A Robust Control Scheme for Grid-Connected Voltage-Source Inverters," *IEEE Trans. Power Electron.*, vol. 58, no. 1, pp. 202-212, 2011.  
 [21] V. Blasko and V. Kaura, "A novel control to actively damp resonance in input *LC* filter of a three-phase voltage source converter," *IEEE Trans. Ind. Appl.*, vol. 33, no. 2, pp. 542-550, Apr. 1997.

- [22] C. Liu, X. Zhang, L. Tan and F. Liu "A novel control strategy of LCL-VSC based on notch concept," in *Proc. of PEDG 2010*, pp.343-346, 2010.
- [23] P.A. Dahono, "A control method to damp oscillation in the input LC-filter," in *Proc. PESC '02*, vol. 4, pp. 1630-5, 2002.
- [24] Y. Tang, P. C. Loh, P. Wang, F. H. Choo and F. Gao, "Exploring inherent damping characteristics of LCL-filters for three-phase grid connected voltage source inverters," *IEEE Trans. Power Electron.*, vol. 27, no. 3, pp. 1433-1443, Mar. 2012.
- [25] D. G. Holmes, T. A. Lipo, B. P. McGrath and W. Y. Kong, "Optimized design of stationary frame three phase AC current regulators," *IEEE Trans. Power Electron.*, vol. 24, no. 11, pp. 2417-2425, Nov. 2009.
- [26] F. Liu, Yan Zhou, S. Duan, J. Yin, B. Liu, F. Liu, "Parameter Design of a Two-Current-Loop Controller Used in a Grid-Connected Inverter System With LCL Filter," *IEEE Trans. Ind. Electron.*, vol. 56, no. 11, pp. 4483-4491, 2009.
- [27] M. Xue, Y. Zhang, Y. Kang, Y. Yi, S. Li, and F. Liu, "Full feed forward of grid voltage for discrete state feedback controlled grid-connected inverter with LCL filter," *IEEE Trans. Power Electron.*, vol. 27, no. 10, pp. 4234-4247, Oct. 2012.